Experimental Hybrid AC/DC-Microgrid Prototype for Laboratory Research

Enrique Espina[1,2], Claudio Burgos-Mellado[3], Juan S. Gómez[1], Jacqueline Llanos[4,1], Erwin Rute[1], Alex Navas F.[1], Manuel Martínez-Gómez[1], Roberto Cárdenas[1], and Doris Sáez[1]
[1]University of Chile, Santiago, Chile. [2]University of Santiago, Santiago, Chile.
[3]PEMC, University of Nottingham, Nottingham, UK.
[4]Universidad de las Fuerzas Armadas ESPE, Sangolqui, Ecuador.
[1]Email: eespina@uchile.cl

Acknowledgments

This work was supported by CONICYT-PCHA/Doctorado Nacional/2017-21171858, 2019-21190961, 2019-21191757, by SENESCYT-CZ03-000368-2018, in part by FONDECYT 1180879 & FONDECYT 1170683, in part by SERC-Chile ANID/FONDAP/15110019, in part by FONDEQUIP EQM130158, and in part by AC3E Basal Project FB0008.

Keywords

≪Hybrid microgrid≫, ≪AC/DC microgrid≫, ≪Experimental prototype≫, ≪Laboratory research≫, ≪Testbed microgrid≫.

Abstract

This paper describes a flexible testbed of a hybrid AC/DC microgrid developed for research purposes. The experimental setup is composed of 3 AC and 6 DC distributed generator units which are emulated by using three-legs inverters and settable output filters. The microgrid architecture allows to validate control schemes upstream of the modulation stage of each inverter, by using real-time targets and Matlab/Simulink interface. Two independent real-time communication networks can be used. The first one is based on optical fibre technology, whereas the second one is an Ethercat communication network. Both of them are used for instrumentation purposes and to implement the primary control level of the microgrid. To implement secondary control schemes into the microgrid (or higher control levels), an additional optical fibre-based network is used, allowing to emulate scenarios with or without communication issues such as latency, data-losses and topology changes. The built microgrid can be splitted into AC-side (3 and/or 4 wires), DC-side and interlinking-side, where both the AC and the DC side can be operated independently, according to the required electrical topology. In this testbed, several control schemes, such as proportional-integral, proportional-resonant or predictive controllers, have been investigated. Realised experimental tests include load changes, plug-and-play and communication issues scenarios.

Introduction

The concept of microgrid (MG) refers to a flexible and modular power generation and distribution system, i.e. distributed generators (DGs) are located near local loads completing an autonomous electrical system, which can operate in either 'grid-connected' or 'islanded' mode [1]. This concept is especially useful when combined with converter-based DG technologies, including Battery Energy Storage Systems (BESS), and the stochasticity of Low-Voltage (LV) conventional distribution networks. MGs have three main architectures depending on their voltage nature, which are: (i) AC, (ii) DC and (iii) hybrid AC/DC. The latter combines the benefits of both MGs through bi-directional interlinking converters (IC). Furthermore, hybrid MGs enhance reliability (as power can be transferred bidirectionally through the IC) while reducing power conversion stages and losses (by up to 30%) [2]. For these reasons, hybrid MGs have become a focus to conduct research at a laboratory level.

(a) Hardware of Triphase® units.

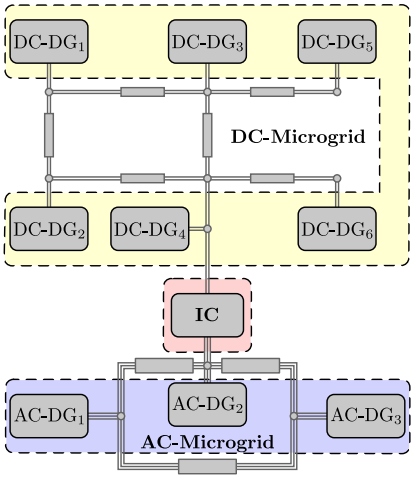

(b) General topology of the implemented hybrid MG.

Fig. 1: Hardware for DGs in Microgrids Control Laboratory, University of Chile.

MG testbeds are set-ups that mimic the real behaviour of a topology in a laboratory environment. These experimental testbeds require flexible platforms to implement embedded real-time control systems. The embedded controllers allow developing strategies capable to preserve the stability and power quality for different electrical or communication topologies. In the literature, there have been reported several MG testbeds, each of them unique in its application and control features [2–8].

The purpose of this paper is to describe the components of the designed MG testbed (located at the MGs Control Laboratory of the University of Chile [9]), explaining the main features developed for coping with the main issues related to the operation of a hybrid MG. A brief explanation about the components of the hybrid MG testbed is addressed. Operation tests are also included for probing the performance of the system when emulating the behaviour of a real MG.

Hardware equipment for Distributed Generator emulation

The emulation of DGs is performed by real-time controlled power units whose manufacturer is the company Triphase® [10], part of National Instruments (NI). Each Triphase® unit consists of inverters connected in a back-to-back configuration through a DC-Link, feeded by the main grid through an isolation transformer. Fig. 1.a shows the Triphase® units conforming the hybrid MG testbed. The control over Triphase® units is executed by real-time targets (RTT) with a unix-based operating system. The control scheme for each Triphase® unit is deployed on the RTT using a MATLAB/Simulink® environment. Instrumentation and control signals of each DG are driven from/to the RTT through an optical or Ethercat real-time network; whereas monitoring information and user triggers are sent from the MATLAB/Simulink® interface to the RTT using a conventional local area network (LAN). This architecture allows to deploy Hardware-in-the-loop (HIL) implementations, to emulate renewable energy resources and load profiles, and to investigate strong MG disturbances such as DGs disconnection/reconnection or losses of communication among controllers.

The testbed's total capacity is 24.0kW (further details are shown in Table I). Fig. 1.b highlights a diagram of the current topology of the complete hybrid MG where the AC-side (in blue), the DC-side (in yellow), and the interlinking converter (in red) are displayed. It is important to notice that this topology is configurable, and it can be modified accordingly to fulfil with the requirements of the research being carried out by the Laboratory. For instance, Fig. 2 shows a 3-wire three-phase isolated MG, implemented in the laboratory to an underway research. A general description of the generation units that compose the hybrid MG and the research benefits that come with this platform are discussed in the sections that follow.

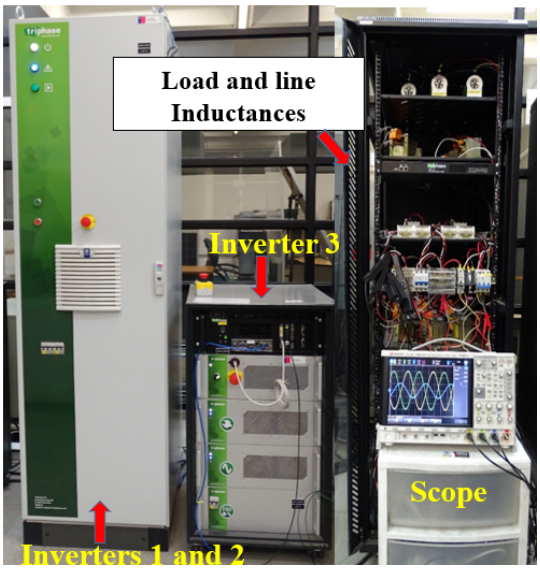

Fig. 2: Example of a 3-phase AC MG implemented in the laboratory for research purpose

Description	DC	AC	IC
# of *DGs*	6	3	1
Nom. Voltage (V)	$50-200$	$50-220^{*}$	-
MG's freq. (Hz)	-	$50-60$	-
Nom. Power ($\frac{kW}{DG}$)	2.5	3.0	3.0
Switch. freq. (kHz)	16		
Comm. rate (Hz)	$10-16000$		

* *Phase-to-neutral RMS voltage*

Table I: Experimental AC/DC-MG, general parameters

Hybrid AC/DC-microgrid Implementation

AC-microgrid

The AC-MG consists of three distributed generation units emulated by using the Triphase® units PM15F120C and PM5F60R, whose maximum powers are 11.5kW and 5.5kW, respectively. The Triphase® unit PM15F120C corresponds to an AC/AC back-to-back converter composed of two inverters at the input and two inverters at the output, where the latter can be configured as three-legged in order to emulate two independent generation units, or it also can be configured as a four-legged inverter, as it is shown in Fig. 3.a. On the other hand, the Triphase® PM5F60R unit is a back-to-back converter with three-phase input and output, which can be used to emulate a third three-phase generation unit, as depicted in Fig. 3.d. Each unit's output can be configured as an LC, LCC, LCL or LCLC filter, depending on whether it operates under voltage source or current source mode, respectively.

The topology of the AC-MG is shown in Fig. 1.b, from which it is observed that the generation units are connected using distribution lines emulated by inductances. Additionally, coupling inductances are connected at the output of the unit filters and three-phase resistive loads are connected to the nodes downstream to carry out load step tests.

Using the AC side, distributed control strategies for isolated MGs presented in [11–13], have been experimentally validated. Whereas the authors of [11] presented a control strategy for the regulation of voltage and frequency using model predictive control, the authors of [12] presented a control scheme able to realise economic dispatch and congestion management in the MG. Furthermore, the authors of [13] proposed a strategy to share imbalances and harmonics in a four-wire droop-controlled MG.

DC-Microgrid

The DC-MG consists of six independent DC distributed generation units emulated by the Triphase® PM15I60F06 unit, whose maximum power is 30.0kW. As shown in Fig. 3.b, this unit consists of two inverters at the input and two inverters at the output, which are connected in back-to-back configuration. Three positive-pole continuous outputs are obtained from each output inverter, while the negative pole of each of them is physically connected to the DC-link negative point. It should be noted that an LC, LCL, LCC or LCLC filter can be configured at the output of each inverter, depending on the operation mode of each converter.

The topology of the DC-MG is shown in Fig. 1.b. There, it can be seen that the units are connected using distribution lines with resistive component and a series inductance to smooth out the variation of

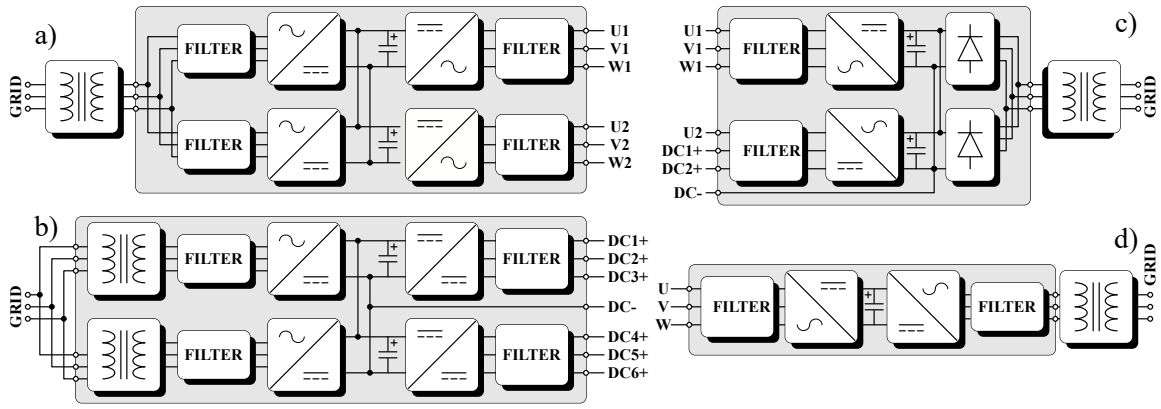

Fig. 3: Hardware configuration of Triphase® Units a) PM15F120C. b) PM15I60F06. c) PM5F42R. d) PM5F60R.

the current. Additionally, a local resistive load is connected after the output filter of each unit to perform connection/disconnection load tests.

Interlinking converter (IC)

The interlink converter which connects the AC-MG and the DC-MG is emulated by the Triphase® PM5F42R unit whose maximum power is 5.5 kW. In a hybrid AC/DC MG the objective of the IC is to control and transfer active power between the AC-side and the DC-side, as well as the possibility of providing reactive power support on the AC-side to contribute to voltage regulation. This Triphase® unit contains a back-to-back converter with a three-phase inverter at the input, and one three-phase inverter at the output. From the latter, there are two continuous positive outputs, while the negative pole of each one is connected to the negative pole of the DC-link.

Currently, this unit is configured as follows: the input inverter allows to control the DC-link voltage and to feed-forwarding control the current/power on the AC-side of the IC, while the inverter at the output allows to control the current/power at the DC-side of the IC. Nevertheless, this unit allows to change the current configuration and to control the DC-link voltage with the DC-side converter. The hardware configuration used in PM5F42R is shown in Fig. 3.c.

Besides the aforementioned application of the Triphase® PM5F42R unit as an interlinking converter, this module can also be used as an active filter (3 or 4-wire configuration) or to control the charge/discharge of batteries at the DC-side. Therefore, the MG implemented in the laboratory also allows to implement an AC-MG with ESS.

Communications between the emulated distributed generation units

The system used for communications among DGs can be described considering the layers of the OSI model. In the physical layer, the communications system is based on optical fibre. The RTTs communicate through an optic fibre ring configuration, as is depicted in Fig. 4.a. In the data-link, network and transport layers, the manufacturer has developed its own communications protocol. In addition to the aforementioned optical ring, a dedicated real-time network is stated among each RTT, its power module and a local distributed power measurement (DPM) module, as it is shown in Fig. 4.b.

As for the upper layers of communication (session, presentation and application), these are done through the Matlab/Simulink® graphical programming interface. The default topology provided by the manufacturer is a master-slave configuration. Although the Triphase® units physically communicate in a certain direction (given by the ring), the connectivity configuration of the DGs is fully customizable. The configuration between each DG is done through the master's program (application layer), allowing simulation of a p2p topology where the master only acts as a bridge to send data packages to any pair of nodes. In this same process, transport delays are added to simulate real distances and conditions in the communication network. Locally, Triphase® models can detect connectivity with neighbours through

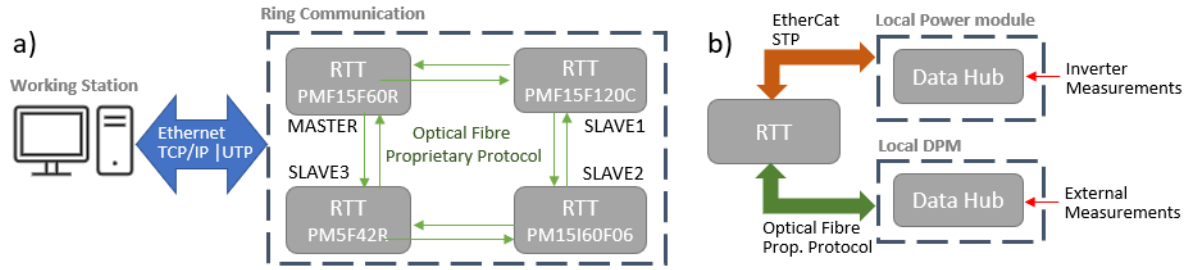

Fig. 4: Communications system of MG testbed. a) Optical fibre ring among RTTs. b) Hardware configuration for each RTT.

communication status bits. Adaptive algorithms can also be introduced for estimating weights of communication links.

Due to the flexibility on the communication network topology and configuration, several communication issues can be easily addressed by the researchers, such as communication delays and communication failures, e.g. time-varying topologies. The performance of the control strategies implemented in the experimental testbed can be monitored in real-time in working stations through a typical local area network (LAN). Furthermore, the experimental hybrid MG can be connected with third party manufacturers, custom made DGs, motor drivers or programmable loads via CAN bus and Modbus protocols.

The flexibility of the experimental platform allows the researchers to implement and analyze in real time complex control strategies with ease, such as robust distributed model predictive control, demand side management and finite-time control strategies.

Operation tests

In this section, experimental results for some of the test realized on the hybrid AC/DC MG are shown. These experimental results depict independent tests for the AC and DC MGs and then, for the whole hybrid MG. Previously reported results comprise the emulation of wind turbines via HIL [14, 15], control schemes for dealing with power quality issues in 4-wire MGs [13, 16, 17], congestion management over AC lines in MGs [12] and, distributed predictive control in AC MGs [11, 18]. Additionally, three papers were submitted to IEEE journals and are currently under review. The first one considers optimal dispatch in AC MGs using distributed predictive control. The second one proposes a global distributed secondary control strategy for hybrid AC/DC-MGs, which is evaluated considering the topology depicted in Fig. 1.b. The third one considers a distributed predictive control strategy for hybrid AC/DC-MGs.

Congestion management and optimal dispatch in AC microgrids

In this section, the experimental dynamic performance of the Distributed Control Strategy for Optimal Dispatch and Congestion Management described in [19] is illustrated and discussed. The MG topology utilized on this work is composed of three converters, three local loads and three power lines (Fig. 5 I).

It can be observed from Fig. 5 II.a and Fig. 5 II.b that the controller is able to successfully restore frequency and resolve congestion after each load perturbation. In specific, Fig. 5 II.a shows how the controller is able to restore the frequency of all DG units to their nominal value (See time-frame 2-5), when the controller is not activated the frequency does not reach the nominal value (see time-frame 1). Likewise, Fig. 5 II.b illustrates that thanks to the correct performance of the controller described in [19], the congestion is quickly eliminated by driving line currents within limits (See time-frames 3 and 5). At time-frame 3, the step-change occurs and line 1 becomes overloaded; however, the distributed congestion controller removes the overloading in less than 3 seconds, which is fast enough to avoid the activation of thermal protections in distribution lines. At time-frame 3, a step-change in load is applied, resulting in an overloading of line 1. Once again, the congestion control is able to resolve the congestion within a few seconds, as shown in Figure 5 II.b in time-frames 3 and 5.

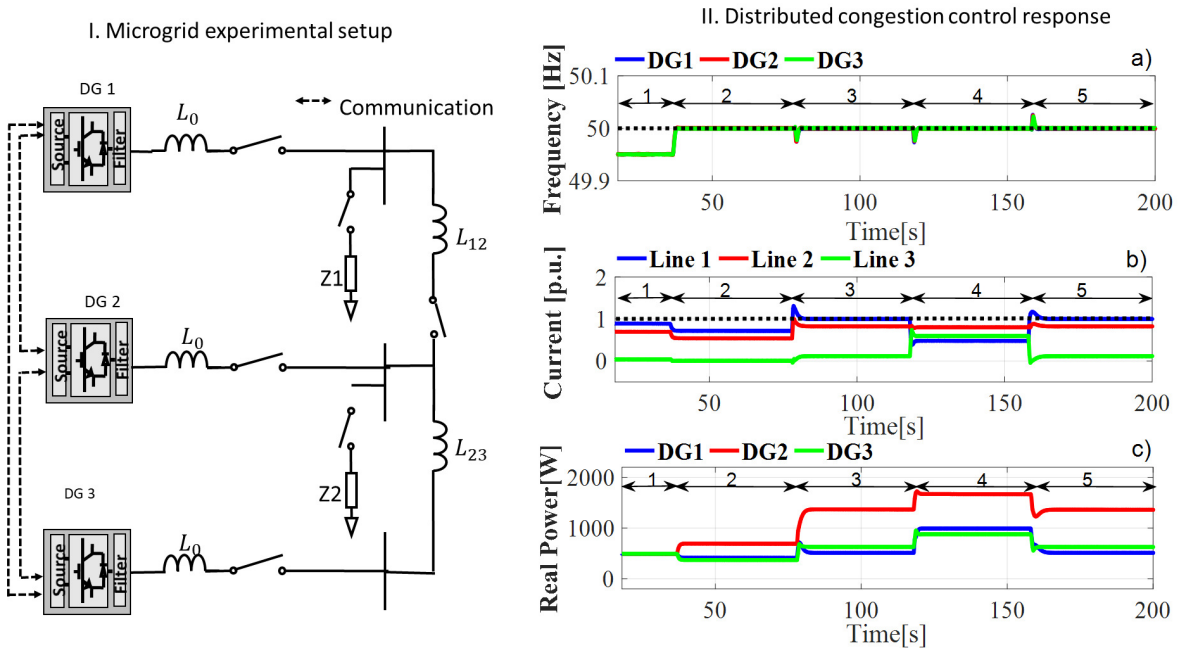

Fig. 5: I. MG experimental setup, II. Distributed congestion control response a) Frequency at each DG, b) Current from the lines, c) Real power injection for each DG

Figure 5 II.c shows the real power generated by each DG unit, at time-frame 1 the real power is shared by the units because only the droop control is activated, also the power injected to the MG is equal in all DG units because their characteristics are the same (see time-frame 1). At time-frames 1 and 2 the load does not change, as it can be seen at time-frame 2 the DG units are re-dispatched considering the operating cost of each unit. The generating cost function ($C_i(P_i) = a_i P_i^2 + b_i P_i + c_i$) of each DG unit is assumed quadratic, the cost parameters of DG are the following [19]: DG1 (a_1=0.444, b_1=0.111, c_1=0), DG2 (a_2=0.264, b_2=0.067, c_2=0), DG3 (a_3=0.5, b_3=0.125, c_3=0).

In order to archive the economic dispatch of the MG. The DG 2 generates more real power than the other units because its operating cost is the lowest, while DG 3 injects less real power than the other DG units because this is more expensive (see time-frame 2 in Fig. 5 II.c). The same performance is shown in the time-frame 4, where the lines are not congested. However, when a control action is required to resolve a congestion (time-frames 2 and 5), the real power injections of DG units are redistributed in order to remove the line overloading based on their different cost functions and participation factors. As can be see, DG 2 generates more real power than the other units because its operating cost is the lowest (see Figure 5II.c time-frames 3 and 5). The good performance of the proposed controller is shown with an increment and a reduction of the load at time-frame 3 to time-frame 5.

Consensus-based Distributed Secondary Control Applied to the Hybrid Microgrid

Fig. 6 shows the behavior of the hybrid MG shown in Fig. 1.b when it is disturbed with simultaneous load impacts at the AC and DC sides, increasing the power flow through the IC. In this test, the AC-side secondary level is controlled using a distributed averaging proportional integral scheme, inspired by [20]. Frequency regulation and active power consensus are merged on one controller, whereas average voltage regulation and reactive power consensus are merged on a second controller. For the DC-side, only one secondary controller, which merges average voltage regulation and active power consensus, is required. In this test, a full meshed communication network is used, which means that each DG in the hybrid MG exchanges information with the other ones at the AC and DC sides.

As it is shown in Fig. 6.a and Fig. 6.b, active and reactive power consensus, as a reason of each DG capacity, are achieved along the test. In a similar way, frequency regulation for AC-side (Fig. 6.f) and average voltage regulation for AC and DC sides are achieved. Note that as the average voltage, instead

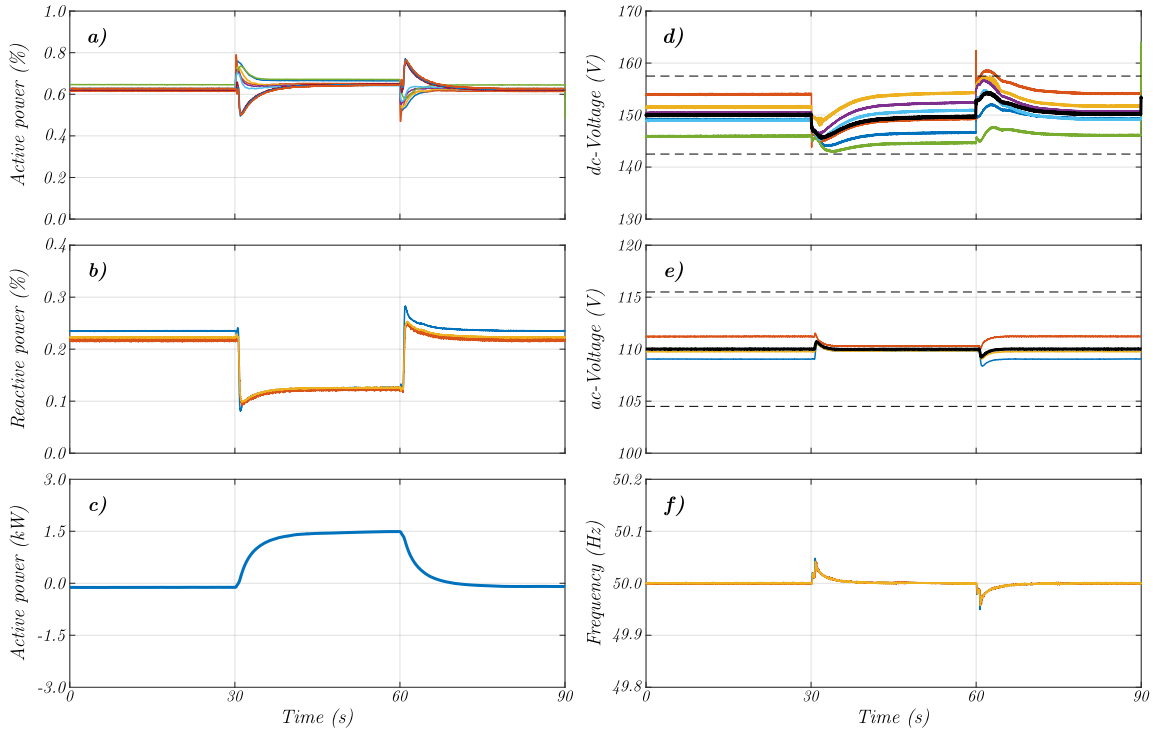

Fig. 6: Variables on the hybrid AC/DC-MG for a load impact test. a) Percentage of active power on each DC-DG and AC-DG. b) Percentage of reactive power on AC-DGs. c) Active power in the IC. d) Voltage on DC-DGs. e) Frequency on AC-DGs. f) Phase-to-neutral RMS voltage on AC-DGs.

of the local voltage for each DG, is regulated, a minor voltage dispersion (less than 5%) is permitted; as shown in Fig. 6.d and Fig. 6.f.

Note that, when the load step disturbs the MG, at $t = 30s$, the power flow through the IC increases (from 0KW to 1.5kW), as shown in Fig. 6.c. Once active power is imported from the AC-side to the DC-side, the IC contributes to the voltage support as well, then both, the reactive power and the voltage dispersion at the AC-side are reduced. When the load is reduced to the initial value, at $t = 60s$, the MG reestablishes the previously described power contribution per DG, preserving the power consensus among the AC and DC generators.

Fault Tolerant Distributed Predictive Control for AC microgrids

In this section a distributed model-based predictive controller (DMPC) is used to improve the plug and play (PnP) capability and the communication latency tolerance in an AC MG. A complete description about the controller synthesis and complementary results are shown in [11] and [18]. The AC MG from the previously described testbed, which is shown in Fig. 5 is used. In this case line L_{13} is arbitrarily disconnected along the whole test.

To test the PnP capability, the DG_3 is disconnected from the MG (at $t = 49s$); disabling its secondary controller. When the failure is cleared, a synchronization sequence is executed only on DG_3, then, it is reconnected to the MG (at $t = 75s$) and its secondary controller re-enabled, as it is shown in Fig. 7.

The results shown that active and reactive power are distributed between DG_1 and $DG2$ when DG_3 fails, but also when it is reconnected to the MG. The adjacency matrix A(t), which represents the communication connectivity, is automatically updated, therefore the consensus terms used in each DMPC are also adjusted. As it is expected, after DG_3 is reconnected, it does not have participation in the power consensus until its secondary controller is enabled.

To test the latency tolerance, a delay is added over each communication path, but the estimated latency used in each controller is preserved. The controller sampling period and the estimated delay are $T_s =$

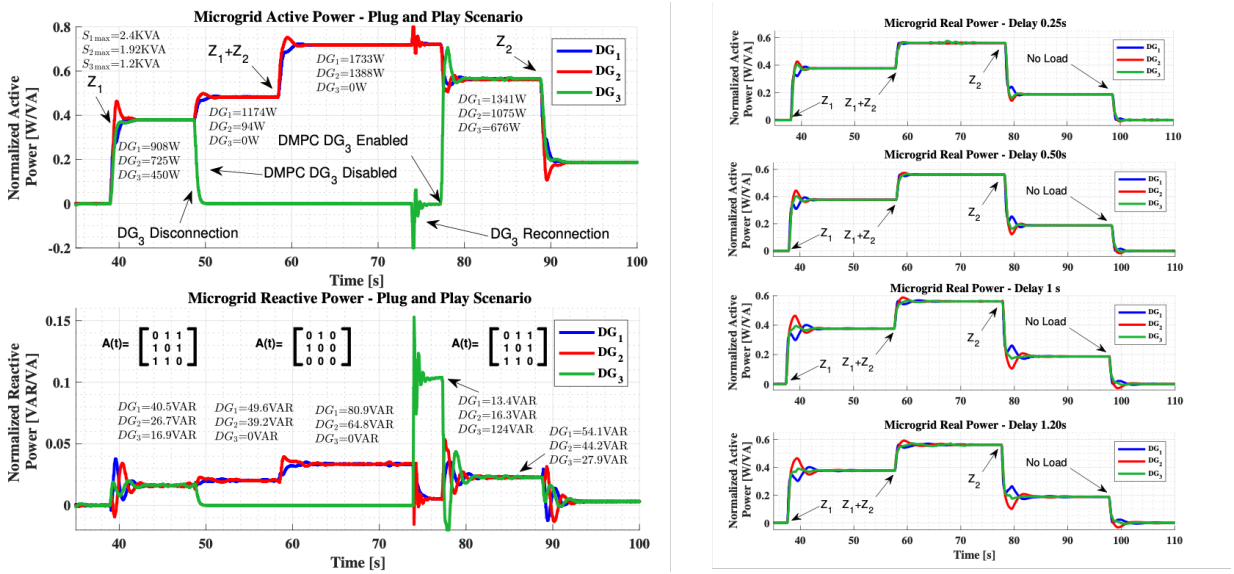

Fig. 7: Active (left-top) and reactive (left-bottom) Power responses in PnP test. Active power response against communication latency (right).

$\hat{\tau}_{ij} = 0.05s$, and the prediction and control horizons are 10 steps ahead. Changes in latency can be caused by issues such as the weather, interference or maintenance frequency, diminishing the communication performance specially in rural/remote areas, where MGs are often used.

From the results, shown in Fig. 7, it is possible to state that the MG response increases its overshoot and its settling time when the communication delay also increases; however, even, the delay is 20-times the sampling period, the control objectives are achieved in the MG. This latency tolerance is related to the prediction horizon, the relation between the rolling horizon scheme and the sampling period and, the delay estimation $\hat{\tau}_{ij}$ included in the optimization problem solved by each controller.

Conclusion

In this paper, a 24kW experimental hybrid AC/DC MG implemented at a laboratory environment has been presented and discussed in detail. The main advantage of the experimental rig is the fact that the control system of units is implemented in Matlab/Simulink environment, and therefore it is not necessary to implement it using programming languages such as C or C++, reducing noticeable the time employed in experimental validation. The experimental system can be configured as AC, DC or hybrid AC/DC MG, providing a wide range of MG topologies to research purposes. Finally, some experimental tests of the system working as a hybrid AC/DC MG were provided. Moreover, some papers published by our research group using this experimental rig have been reported and discussed.

References

[1] Office of Electricity Delivery and Energy Reliability, "Summary Report : 2012 DOE Microgrid Workshop," Department of Energy - USA, Tech. Rep., 2012.

[2] A. A. Jabbar, A. Y. Elrayyah, M. Z. Wanik, A. P. Sanfilippo, and N. K. Singh, "Development of Hybrid AC/DC Laboratory-scale Smart Microgrid Testbed with Control Monitoring System Implementation in LabVIEW," in *IEEE Grand Int. Conf. Expo. Asia (GTD Asia)*, 2019, pp. 889–894.

[3] E. Hossain, E. Kabalci, R. Bayindir, and R. Perez, "Microgrid testbeds around the world: State of art," *Energy Conversion and Management*, vol. 86, pp. 132–153, 2014.

[4] G. Turner, J. P. Kelley, C. L. Storm, D. A. Wetz, and W. J. Lee, "Design and active control of a microgrid testbed," *IEEE Trans. Smart Grid*, vol. 6, no. 1, pp. 73–81, 2015.

[5] A. Tak and T. S. Ustun, "Design of a generic microgrid testbed with novel control and smart technologies," in *3rd Int. Renewable Sustain. Energy Conf. (IRSEC)*, 2016.

[6] M. H. Cintuglu, O. A. Mohammed, K. Akkaya, and A. S. Uluagac, "A Survey on Smart Grid Cyber-Physical System Testbeds," *IEEE Commun. Surveys Tuts.*, vol. 19, no. 1, pp. 446–464, 2017.

[7] M. H. Cintuglu, T. Youssef, and O. A. Mohammed, "Development and application of a real-time testbed for multiagent system interoperability: A case study on hierarchical microgrid control," *IEEE Trans. Smart Grid*, vol. 9, no. 3, pp. 1759–1768, 2018.

[8] Z. Cheng and M. Y. Chow, "The development and application of a DC microgrid testbed for distributed microgrid energy management system," in *44th Annu. Conf. Ind. Electron. Soc. (IECON)*, 2018, pp. 300–305.

[9] Microgrids Control Laboratory, University of Chile. [Online]. Available: http://microgrids.ing.uchile.cl/

[10] Triphase. [Online]. Available: https://triphase.com/products/

[11] J. S. Gómez, D. Sáez, J. W. Simpson-Porco, and R. Cárdenas, "Distributed predictive control for frequency and voltage regulation in microgrids," *IEEE Trans. Smart Grid*, pp. 1–1, 2019.

[12] J. Llanos, J. Gómez, D. Sáez, D. Olivares, and J. Simpson-Porco, "Economic dispatch by secondary distributed control in microgrids," in *21st Eur. Conf. Power Electron. and Appl. (EPE)*, 2019, pp. P.1–P.10.

[13] C. Burgos-Mellado, J. Llanos, R. Cárdenas, D. Sáez, D. E. Olivares, M. Sumner, and A. Costabeber, "Distributed control strategy based on a consensus algorithm and on the conservative power theory for imbalance and harmonic sharing in 4-wire microgrids," *IEEE Trans. Smart Grid*, pp. 1–1, 2019.

[14] Y. Muñoz-Jadán, M. Espinoza-Bolaños, F. Donoso Merlet, R. Hidalgo-León, G. Soriano Idrovo, and P. Jcome-Ruz, "Hardware-in-the-loop for wind energy conversion with resonant current control and active damping," *IEEE Lat. Am. Trans.*, vol. 17, no. 07, pp. 1146–1154, 2019.

[15] Y. Muñoz-Jadán, "Emulación de un aerogenerador conectado a la red a través de un sistema experimental Back-to-Back mediante la técnica "Hardware In The Loop"," Master's thesis, University of Chile - Electrical Engineering Department, 2016. [Online]. Available: http://repositorio.uchile.cl/handle/2250/143852

[16] C. Burgos-Mellado, R. Cárdenas, D. Sáez, A. Costabeber, and M. Sumner, "A control algorithm based on the conservative power theory for cooperative sharing of imbalances in four-wire systems," *IEEE Trans. Power Electron.*, vol. 34, no. 6, pp. 5325–5339, 2019.

[17] C. Burgos-Mellado, "Control strategies for improving power quality and PLL stability evaluation in microgrids," Ph.D. dissertation, University of Chile - Electrical Engineering Department, 2019. [Online]. Available: http://repositorio.uchile.cl/handle/2250/170135

[18] J. S. Gómez, "Distributed predictive control for frecuency and voltage regulation in microgrids," Ph.D. dissertation, University of Chile - Electrical Engineering Department, 2020. [Online]. Available: http://repositorio.uchile.cl/handle/2250/173842

[19] J. Llanos, D. E. Olivares, J. W. Simpson-Porco, M. Kazerani, and D. Sáez, "A novel distributed control strategy for optimal dispatch of isolated microgrids considering congestion," *IEEE Trans. Smart Grid*, vol. 10, no. 6, pp. 6595–6606, 2019.

[20] J. W. Simpson-Porco, Q. Shafiee, F. Dorfler, J. C. Vasquez, J. M. Guerrero, and F. Bullo, "Secondary Frequency and Voltage Control of Islanded Microgrids via Distributed Averaging," *IEEE Trans. Ind. Electron.*, vol. 62, no. 11, pp. 7025–7038, 2015.